A&A 378, 653–667 (2001)
DOI: 10.1051/0004-6361:20011212


Astronomy & Astrophysics

# Visible and near-IR observations of transneptunian objects
## Results from ESO and Calar Alto Telescopes⋆

H. Boehnhardt[1], G. P. Tozzi[2], K. Birkle[3], O. Hainaut[1], T. Sekiguchi[1], M. Vair[1], J. Watanabe[4], G. Rupprecht[5], and The FORS Instrument Team[6,7,8]

[1] European Southern Observatory ESO, Alonso de Cordova 3107, Santiago de Chile, Chile
e-mail: ohainaut@eso.org; tsekiguc@eso.org; mvair@eso.org
[2] Osservatorio Astrofisico di Arcetri, Largo E. Fermi, 50125 Firenze, Italy
e-mail: tozzi@arcetri.astro.it
[3] Max-Planck-Institut für Astronomie, Königstuhl 17, 69117 Heidelberg, Germany
e-mail: birkle@mpia-hd.mpg.de
[4] National Astronomical Observatory of Japan, Osawa, Mitaka, Tokyo 181-8588, Japan
e-mail: watanabe@nao.jp.ac
[5] European Southern Observatory ESO, Karl-Schwarzschild-Str. 2, 85748 Garching, Germany
e-mail: grupprec@eso.org
[6] Landessternwarte Heidelberg, Königstuhl, 69117 Heidelberg, Germany
e-mail: iappenze@lsw.uni-heidelberg.de (FORS Principle Investigator)
[7] Universitäts-Sternwarte Göttingen, Geismarlandstr. 11, 81679 Göttingen, Germany
[8] Universitäts-Sternwarte München, Scheinerstr. 1, 81679 München, Germany

Received 10 January 2001 / Accepted 21 August 2001

**Abstract.** We present visible ($BVRI$) and near-IR ($JHK_s$) broadband photometry and visible low-dispersion spectroscopy of Transneptunian Objects (TNOs) and Centaurs. In total, 16 TNOs and 1 Centaur were observed over the past two years at ESO telescopes in La Silla and Paranal in Chile as well as at the Calar Alto Observatory in Spain. The sample consists of objects measured for the first time and those for which comparison data is available from literature. The targets were: 1992QB1, 1993RO, 1994EV3, 1995HM5, 1995SM55, 1996RQ20, 1996TL66, 1996TO66, 1996TP66, 1997CQ29, 1997CS29, 1998HK151, 1998TF35, 1998VG44, 1998WH24, 1998XY95, 1999TC36. The spectra of 5 TNOs (1995SM55, 1996TO66, 1997CQ29, 1997CS29, 1998HK151) show almost constant gradients over the visible wavelength range with only marginal indication for a flatter slope beyond 750–800 nm. The photometric colour gradients obtained quasi-simultaneously are in good agreement with the spectral data. This suggests that in general photometric colour gradients are a valuable diagnostic tool for spectral type classification of TNOs. The photometric study revealed a number of new objects with neutral and red colours. For re-measured objects the published broadband colours were – in general – confirmed, although a few remarkable exceptions exist. Two TNOs appear to be outlyers according to the available broadband colours: 1993EV3 and 1995HM5. 1995SM55 is the bluest TNO measured so far. No clear global correlation between $V-I$ colour and absolute $R$ filter brightness of our TNO targets is found. However, the data for the 5 brightest TNOs (brighter than 5 mag absolute magnitude) could also be interpreted with a linear increase of $V-I$ colour by about 0.75 mag per brightness magnitude. The colour-colour diagrams show continuous reddening of the TNOs in $V-R$ vs. $B-V$, $R-I$ vs. $B-V$ and $R-I$ vs. $V-R$. The bimodality suggested from earlier measurements of Tegler & Romanishin (1998) is not confirmed. According to our colour gradient statistics (number of objects per gradient interval) most of the TNOs have surface reddening between 0 and 40%/100 nm. For the Cubewanos the major population falls between 20–40%/100 nm. The Plutinos and Centaurs show a bifold grouping, i.e. a neutral/slightly reddish group (reddening <20%/100 nm) and a red group (reddening 30–40%/100 nm). The statistical significance of the various populations found is suffering – for the Centaurs and scattered disk objects very severely – from the small number of objects measured. However, the diversity of the reddening distribution of Centaurs/Plutinos and Cubewanos, if confirmed by new observations, may indicate a different balancing of resurfacing processes for these object types: for instance, for Centaurs a possibility is that re-condensed frost from coma activity may be dominant over impact re-surfacing and high energy surface processing.

**Key words.** transneptunian objects – cubewanos – plutinos – scattered disk objects – Centaurs – photometry – spectroscopy

*Send offprint requests to*: H. Boehnhardt,
e-mail: hboehnha@eso.org

⋆ Based on observations performed at the European Southern Observatory at La Silla and Paranal in Chile and at the German Spanish Astronomical Centre at Calar Alto in Spain, operated by the Max-Planck-Institut für Astronomie, Heidelberg, jointly with the Spanish National Commission for Astronomy.

## 1. Physical properties of TNOs and Centaurs

The number of discovered Transneptunian Objects (in the following TNOs) and of Centaurs has steadily – over the past 3 years even rapidly – increased. At present more than 400 TNOs and about 25 Centaurs are known, a significant part still with uncertain orbits.

TNOs are believed to populate the Edgeworth-Kuiper Belt (which was first hypothesised by Edgeworth 1949 and Kuiper 1951). TNOs are classified in three dynamical groups (Levison 2001): the Plutinos are captured in stable orbits in the 2:3 resonance with Neptune. The Cubewanos occupy the orbits between the Plutinos and the 1:2 resonance with Neptune. Scattered disk objects are found in highly elliptical orbits with semi-major axes between about 40 and several hundreds Astronomical Units. They appear to be TNOs that are scattered out of the Edgeworth-Kuiper Belt by the giant planets.

Centaurs are believed to be TNOs which migrated towards the Sun by gravitational interaction with the major planets. They may finally become short period comets as member of the Jupiter family or they may be scattered (as long-period or Oort cloud comets) into the outskirts of the Solar System (Levison 2001). A recent analysis of the comet radius distribution further supports this evolution track: Meech and collaborators (priv. comm.) showed that the observed radii are not following a power law as it would be expected if the short-period comets were directly injected in the inner Solar System by a collision process.

Since the TNOs never came really close to the Sun, they are considered to represent an old and physico-chemically unaltered population of Solar System bodies. In this respect, TNOs may be even more pristine than Centaurs and short-period comets which both show gas and dust emission acitivity and which may thus no longer have an original surface layer constitution (Meech et al. 1997). The knowledge of physical parameters of TNOs and Centaurs suffers from the faintness of the objects which calls for observations with large telescopes on the ground or for observations with the Hubble Space Telescope (HST).

Size estimates exist from coarse single or two colour photometry obtained by search programs. More accurate multi-colour photometry of about 50 TNOs in the visible wavelength range is published, near-IR colours of TNOs are rarer (about 15 objects published). 6 Centaurs have visible and near-IR broadband colours measured, a few more objects of at least *BVRI* colours measured.

For a more recent compilation of the published photometry data of TNOs and Centaurs see Barucci et al. 1999a and 1999b (even though an update of the tables with the latest results is needed – see below).

Obviously, TNOs and Centaurs exhibit different reddening in their broadband colours which may be indicative for different physical processing of their surfaces. At present, the existence of two TNO groups with distinct colours appears to be controversial (Tegler & Romanishin 1998, 2000; Davies et al. 2000; Barucci et al. 2000; Trujillo et al. 2000). Recently, a paper by Barucci et al. (2001) outlined a new approach for the taxonomic classification of TNOs and Centaurs that follows the statistical analysis for the detection of asteroid types using photometric data.

Spectra of a handful TNOs are available in literature: while the visible spectra of TNOs (Jewitt & Luu 1998) appear featureless, absorption bands of water and hydrocarbon ices were found in one TNO in the near-IR (1996TO66; Brown et al. 1997, 1999; Noll et al. 2000).

The Centaurs have either neutral or very red colours. Spectroscopy (5 objects published, Barucci et al. 1999a) in the visible and near-IR revealed mostly reflectance spectra, but in one case also CN gas emission (Meech et al. 1997). $H$ and $K$ band water ice absorptions were also reported (Cruikshank et al. 1998).

Hitherto, the existing database did not yet allow to draw firm conclusions on a generally accepted taxonomic classification scheme for TNOs and Centaurs.

In the following sections we present photometry (visible and near-IR) of 16 TNOs and 1 Centaur as well as visible spectra of 5 TNOs. The observations are part of a co-ordinated program for the exploration of physico-chemical properties of TNOs and Centaurs, executed by our group at observatories in Chile, Spain and USA.

## 2. Observations at ESO VLT, NTT and at Calar Alto

The observations were collected in the visible and near-infrared (near-IR) wavelength ranges during 5 runs between 1998 and early 2000 at the ESO observatories in La Silla and Paranal and at the Calar Alto Observatory in Spain (Table 1). In La Silla we used the 3.6 m New-Technology-Telescope (NTT) equipped with the near-IR instrument SOFI. At Paranal we used the 8.2 m UT1 Telescope of the ESO Very Large Telescope VLT. In 1998 UT1 was equipped with the VLT Test Camera (TC), in 1999 we used the FORS1 instrument. Both the TC and FORS1 work in the visible wavelength range. The Calar Alto data were also collected in the visible wavelength range at the 3.5 m telescope using the MOSCA focal reducer. The filters and wavelength ranges used during the various observing runs are listed in Table 1. Details on the telescopes and instruments can be found on the web pages of these observatories. The log of the observations is given in Tables 2 and 3. Note: at the ESO telescopes we used filters from the Bessell system for imaging, while at Calar Alto Johnson-type *BVI* filters and a special $R$ passband filter with steep cut-off near 750 nm were installed. The objects were selected with the goal to contribute new and/or improved broadband colours in the visible and near-IR wavelength range for the taxonomic characterisation and classification of TNOs and Centaurs.

The spectroscopy part focused on a subset of the objects imaged with broadband filters. The spectra (all taken with FORS1 at the VLT) were obtained either

**Table 1.** Telescope and instruments for the TNO/Centaurs observations.

| Observ. Period | Observatory<br>Telelescope + Instrument | Filters<br>Spectral Range (nm) | Imaging Objects<br>Spectroscopy Objects |
|---|---|---|---|
| 24–26 Aug. 1998 | ESO Paranal<br>VLT UT1 + TC | img.: *BVRI* (Bessell) | img.: 1993RO, 1996TL66, 1996TP66 |
| 19–20 March 1999 | ESO La Silla<br>3.6 m NTT + SOFI | img: $JHK_s$ | img.: 1995HM5, 1997CQ29, 1997CS29 |
| 13–15 May 1999 | ESO Paranal<br>VLT UT1 + FORS1 | img.: *VRI* (Bessell)<br>spec.: 590–1000 | img.: 1994EV3, 1997CQ29, 1998HK151<br>spec.: 1997CQ29, 1998HK151 |
| 2–6 Dec. 1999 | ESO Paranal<br>VLT UT1 + FORS1 | img.: *BVRI* (Bessell)<br>spec.: 350–1000 | img.: 1992QB1, 1995SM55, 1996RQ20, 1996TO66, 1997CS29<br>spec.: 1995SM55, 1996TO66, 1997CS29 |
| 3–6 Jan. 2000 | Calar Alto<br>3.5 m + MOSCA | img.: *BVRI* (Johnson+special) | img.: 1997CS29, 1998TF35, 1998VG44, 1998WH24, 1998XY95, 1999TC36 |

Notations: img.: imaging, spec.: spectra in given wavelength range.

immediately before or after the filter imaging of the respective objects.

All images and spectra were taken under photometric conditions. During imaging the telescopes were used in sidereal tracking/auto-guiding mode. During spectroscopy differential tracking/auto-guiding was applied in order to keep the objects on the 1″ wide slit.

Brightness variations due to rotation of the objects can happen in time intervals as short as a few hours. At the VLT all three or four colours *(B)VRI* of the objects were measured within a short time interval (typically within 20–25 min) at least in one night in order to minimise possible brightness variations due to rotation. The 3.5 m Calar Alto photometry had longer execution times per object. Therefore, in most cases sequences of consecutive exposures in *RBRVIR* filters were used for the sampling of the rotation variability.

The near-IR images were taken through $JHK_s$ filters. A similar strategy as of long lasting *BVRI* sequence was used during the $JHK_s$ exposure series. Random jitter offsets of the telescope were applied during the filter exposure series.

In addition to the object exposures also photometric and spectrophotometric standard stars, flatfield, arc spectra and bias exposures were taken as needed for the calibrations of the data.

## 3. Data processing

In the following subsections the data reduction steps are described separately for imaging photometry in the visible and near-IR as well as for visible spectroscopy.

### 3.1. Visible imaging data: TC, FORS1 and MOSCA

**TC:** since these exposures are part of the VLT UT1 Science Verification (SV) Program, we used the completely reduced images as provided by the SV team (for the reduction steps applied see Giacconi et al. 1999). A small additional work was necessary to identify the TNOs in the reduced images and to obtain the brightness values of the objects in the various filters. This step of the data reduction is described in Hainaut et al. (2000b).

**FORS1 and MOSCA:** basic reduction steps – the usual CCD "cosmetic" data reduction, i.e. bias subtraction, flat field correction and cosmic ray filtering, was at first applied to all the object frames (science objects and standard stars). As bias image, the median of all bias images taken at the beginning and at the end of the nights was used, since no significant changes were found from the frames taken at different times. As flat field images we used the average of several twilight sky images, normalised to 1. To reduce the cosmic ray signatures we filtered the bias and flat field corrected object images with a 3×3 pixels wide median filter. The difference between unfiltered and filtered images showed that no other small-scale structures, but only cosmic ray events were erased from the object images. Sky correction was performed by subtracting a first order polynomial sky approximation computed from the pixel areas containing no stars.

Object identification – the TNOs/Centaurs were then identified by blinking two images recorded at different times. As we observed only objects whose orbit is well known, this ensures proper identification.

Photometry – to measure the magnitude of the TNOs in the reduced FORS1 images, several procedures were applied. The first one was the measurement of the total counts in an annulus of thickness equal to 1 pixel versus the annulus radius. This function should start at 0 for an annulus radius equal to zero, then reach a maximum and decrease to zero again at a certain distance depending on the seeing. It allows at the same time to check the possible presence of residual sky flux in the data (i.e. if skylight is present, the flux does not tend to zero for larger annuli), and to measure the point-spread-function (PSF) of the objects. The integral of this function over the object PSF gives the total counts recorded for each TNO. The second method used the classical magnitude measurements in a synthetic aperture (with the sky measured in a surrounding annulus removed). Third, the fitting of the objects with a two-dimensional Gaussian and the successive calculation of the counts from the measured Gaussian parameters was applied. Usually, the results of all three methods agreed within small margins, much smaller than the photon noise errors.

**Table 2.** Log and results of the TNO/Centaur observations: La Silla and Paranal. In case of multiple exposures within *RBRVIR* filter sequences the mid exposure time and average filter brightness is given. Imaging data are indicated by filter designation ($BVRIJHK_s$ in column Filter/Spectrum), for spectra the spectral range is listed in the same column. All magnitudes apply for the Bessell filter system.

| Object<br>Tel.+Inst. | Date<br>(UT) | Exp.Time<br>(s) | Filter/<br>Spectrum | Brightness<br>(mag) | Error<br>(mag) |
|---|---|---|---|---|---|
| **1992QB1** | 1999 Dec. 05.022 | 300+400 | $V$ | 23.69 | 0.08 |
| UT1+FORS1 | 05.026 | 300+400 | $I$ | 22.53 | 0.07 |
| | 05.031 | 600 | $B$ | 24.69 | 0.18 |
| | 05.039 | 400 | $R$ | 23.09 | 0.06 |
| **1993RO** | 1998 Aug. 24.350 | 600 | $V$ | 24.37 | 0.08 |
| UT1+TC | 24.402 | 600 | $R$ | 23.63 | 0.08 |
| | 24.460 | 600 | $I$ | 23.15 | 0.08 |
| **1994EV3** | 1999 May 13.989 | 300 | $V$ | 23.91 | 0.13 |
| UT1+FORS1 | 13.993 | 300 | $R$ | 23.65 | 0.15 |
| | 13.997 | 600 | $I$ | 22.85 | 0.13 |
| **1995HM5** | 1999 Mar. 20.300 | 3120 | $J$ | 22.39 | 0.29 |
| NTT+SOFI | 20.320 | 2160 | $H$ | 21.21 | 0.37 |
| **1995SM55** | 1999 Dec. 02.026 | 300 | $V$ | 20.54 | 0.03 |
| UT1+FORS1 | 02.030 | 300 | $I$ | 19.89 | 0.03 |
| | 02.035 | 300 | $B$ | 21.22 | 0.05 |
| | 02.041 | 90 | $R$ | 20.28 | 0.03 |
| | 02.045 | 1200 | 590–1000 nm | Fig. 1 | red only |
| **1996RQ20** | 1999 Dec. 04.031 | 200+400 | $R$ | 22.92 | 0.05 |
| UT1+TC | 04.034 | 300 | $V$ | 23.60 | 0.08 |
| | 04.038 | 400 | $I$ | 22.34 | 0.08 |
| | 04.044 | 600 | $B$ | 24.49 | 0.12 |
| **1996TL66** | 1998 Aug. 24.250 | 600 | $B$ | 21.81 | 0.07 |
| UT1+TC | 24.260 | 600 | $V$ | 21.46 | 0.06 |
| | 24.270 | 600 | $R$ | 20.83 | 0.06 |
| | 24.282 | 600 | $I$ | 20.46 | 0.07 |
| **1996TO66** | 1999 Dec. 03.020 | 200 | $V$ | 21.62 | 0.03 |
| UT1+FORS1 | 03.024 | 200 | $I$ | 20.91 | 0.04 |
| | 03.027 | 300 | $B$ | 22.18 | 0.06 |
| | 03.031 | 100 | $R$ | 21.14 | 0.03 |
| | 03.035 | 2x1200 | 350–1000 nm | Fig. 1 | blue+red (1) |
| **1996TP66** | 1998 Aug. 24.332 | 600 | $B$ | 22.89 | 0.08 |
| UT1+TC | 24.341 | 600 | $V$ | 21.86 | 0.06 |
| | 24.353 | 600 | $R$ | 21.27 | 0.06 |
| | 24.365 | 600 | $I$ | 20.62 | 0.07 |
| **1997CQ29** | 1999 Mar. 20.142 | 2400 | $J$ | 21.68 | 0.18 |
| NTT+SOFI | 20.145 | 1920 | $H$ | 21.02 | 0.34 |
| UT1+FORS1 | 1999 May 13.975 | 300 | $V$ | 23.53 | 0.11 |
| | 14.991 | 2x180 | $V$ | 23.91 | 0.11 |
| | 14.973 | 300 | $R$ | 23.20 | 0.08 |
| | 14.977 | 600 | $I$ | 22.59 | 0.11 |
| | 15.007 | 3600 | 590–1000 nm | Fig. 1 | red only |
| **1997CS29** | 1999 Mar. 20.060 | 720 | $J$ | 20.27 | 0.10 |
| NTT+SOFI | 20.060 | 1440 | $H$ | 19.96 | 0.12 |
| | 20.080 | 1440 | $K_s$ | 19.68 | 0.20 |
| UT1+FORS1 | 1999 Dec. 05.300 | 2x200 | $R$ | 21.27 | 0.04 |
| | 05.303 | 400 | $I$ | 20.73 | 0.03 |
| | 05.309 | 500 | $B$ | 22.88 | 0.06 |
| | 05.318 | 250 | $V$ | 21.99 | 0.05 |
| | 05.325 | 1246 | 350–1000 nm | Fig. 1 | blue+red |
| **1998HK151** | 1999 May 14.302 | 300 | $V$ | 22.12 | 0.03 |
| UT1+FORS1 | 15.243 | 2x300 | $V$ | 22.07 | 0.03 |
| | 14.310 | 300 | $R$ | 21.62 | 0.03 |
| | 14.314 | 600 | $I$ | 21.20 | 0.05 |
| | 15.242 | 600 | $I$ | 21.21 | 0.04 |
| | 15.258 | 3600 | 590–1000 nm | Fig. 1 | red only |

Note (1): for 1996TO66 another "red only" spectrum (590–1000 nm) was taken in order to check the contamination of the second order overlap in the red part of the "red+blue" spectrum of this object.

From the measured magnitude of the standard stars, after the application of the instrumental colour and air mass corrections (for detailed information see the ESO VLT Quality Control web page `http://www.eso.org/observing/dfo/quality/`), the zero-points for the nights were computed. With these zero-points and with first order measurements of objects' colours, the magnitudes of the TNO (see Tables 2 and 3) were obtained applying the quoted colour and air mass corrections. The measurement errors given in these tables are the quadratic combination of the photometric and calibration errors. The resulting magnitudes are in

**Table 3.** Log and results of the TNO/Centaur observations: Calar Alto. In case of multiple exposures within *RBRVIR* filter sequences the mid exposure time and average filter brightness is given. Imaging data are indicated by filter designation ($BVRIJHK_s$ in column Filter/Spectrum), for spectra the spectral range is listed in the same column. All magnitudes apply for the Bessell filter system.

| Object<br>Tel.+Inst. | Date<br>(UT) | Exp.Time<br>(s) | Filter/<br>Spectrum | Brightness<br>(mag) | Error<br>(mag) |
|---|---|---|---|---|---|
| **1997CS29** | 2000 Jan. 04.057 | 600 | *V* | 22.17 | 0.05 |
| 3.5 m+MOSCA | 04.067 | 2 × 450 | *I* | 20.72 | 0.05 |
| | 04.069 | 3 × 600 | *R* | 21.39 | 0.03 |
| | 04.092 | 1200 | *B* | 23.20 | 0.06 |
| **1998TF35** | 2000 Jan. 04.978 | 600 | *V* | 22.26 | 0.05 |
| 3.5 m+MOSCA | 04.998 | 2 × 600 | *R* | 21.55 | 0.03 |
| | 05.000 | 2 × 450 | *I* | 20.98 | 0.09 |
| | 05.020 | 1200 | *B* | 23.28 | 0.10 |
| **1998VG44** | 2000 Jan. 05.940 | 600 | *V* | 21.75 | 0.03 |
| 3.5 m+MOSCA | 05.955 | 3 × 600 | *R* | 21.14 | 0.03 |
| | 05.977 | 1500 | *B* | 22.68 | 0.04 |
| | 06.004 | 2 × 450 | *I* | 20.37 | 0.07 |
| **1998WH24** | 2000 Jan. 03.967 | 1200 | *B* | 22.39 | 0.04 |
| 3.5 m+MOSCA | 03.988 | 600 | *V* | 21.56 | 0.04 |
| | 03.994 | 2 × 600 | *R* | 20.92 | 0.02 |
| | 04.000 | 2 × 450 | *I* | 20.53 | 0.04 |
| **1998XY95** | 2000 Jan. 05.061 | 900 | *V* | 23.40 | 0.12 |
| 3.5 m+MOSCA | 05.071 | 2 × 600 | *R* | 22.75 | 0.07 |
| | 05.080 | 3 × 450 | *I* | 21.98 | 0.14 |
| | 05.123 | 1500 | *B* | 24.33 | 0.20 |
| **1999TC36** | 2000 Jan. 04.799 | 600 | *B* | 21.71 | 0.03 |
| 3.5 m+MOSCA | 04.815 | 600 | *V* | 20.75 | 0.03 |
| | 04.822 | 2 × 600 | *R* | 20.05 | 0.02 |
| | 04.829 | 2 × 450 | *I* | 19.47 | 0.03 |

the Bessell filter system as defined in Landolt (1992). Generally, apart from the relatively bright objects, the calibration errors are negligible in comparison with the photometric ones. Regarding the photometric errors the largest source is produced by the sky noise, even in the *V* band where the sky intensity is at minimum. For that reason, to avoid any possible source of systematic errors, it is important to subtract the sky background correctly and to measure the total counts in the smallest possible aperture. In our case the aperture radius varied from 6 to 10 pixels, depending on the seeing present at the time of the observation (note: the diameter for the photometry was larger – by a factor of about 3 – than the full-width-at-half-maximum *FWHM* of the object images which is typically taken as a measure for the image quality).

The MOSCA data was processed in the same way as the FORS1 ones except for the following steps: (1) for each colour the extinction values of the site were determined from standard star images taken every night in the same filter at different air masses. (2) the colour coefficients were obtained from the same standard star data using a linear correction term for $R-I$. This colour transformation took care of the transition of the instrumental colours in the Johnson/special filter set used for the observations into the Bessell filter system needed for the scientific analysis of the results. (3) we applied aperture photometry measurements only as described in the second method of the FORS1 reduction process. For each object the aperture radius of the measurement series varied between 1 and 4 sigma of the PSF.

### 3.2. Infrared data

**SOFI:** basic reduction steps – also for the NTT/SOFI infrared observations the standard procedure for infrared data reduction was applied. First of all, the flat field response for each band was obtained as difference of dome exposures taken with light on and off, normalised to 1. SOFI's bias changes with the illumination level; this was taken into account using additional on-off flatfields obtained after slightly moving the cold mask of the instrument in the beam. This provides a small region where the proper bias correction can be measured. In this way the bias and background contribution of the telescope were taken into account. Then from each observing sequence of the objects a master sky frame was obtained as median of several frames recorded with the telescope pointing always in slightly different positions (jitter images). Finally, the reduced frames were computed as difference of a single object frame minus the sky one, divided by the flat field frame. In this way the sky contribution, the bias and the possible telescope background were also subtracted from the resulting frame.

Object identification – since a single object frame had a typical exposure time of the order of 1 min, the faint TNOs were not easily visible in these images. Therefore, all frames were re-aligned to the computed position of the TNOs using the background stars present in the field and the predicted proper motion of the TNOs. The median of all the aligned images gave an image with the TNO well visible and the background stars dimmed (depending on the TNO proper motion, the length of the exposure and the brightness of the field stars).

**Table 4.** TNO/Centaur absolute brightness, radii, colours and spectral gradients – ESO La Silla, ESO Paranal, Calar Alto. The objects are listed according to designation. The table lists for each object:
- The object designation and the dynamical type (Plutino, Cubewano, Scattered = scattered disk object, Centaur).
- The absolute $R$ filter magnitude $M_R$ (except for 1995HM5 which is based on the $J$ filter brightness).
- The equivalent radius derived from the $R$ filter brightness (except for 1995HM5 which is based on the $J$ filter brightness) for an assumed albedo of 0.04.
- The colours of the objects in a set of cardinal filters ($B-V$, $V-R$, $R-I$, $J-H$, $H-K_s$). The photometric errors of the colours are given in the second line (calculated by standard error propagation from the measurement errors for each filter).
- The colour ($B-I$ and $V-I$) gradients according to Eq. (1) as well as the gradient measured in the reflectance spectra (if available).
- The photometric type of the objects classified according to the colour gradient statistics. Bluish: gradient <0[%/100 nm]; neutral to slightly red: gradient 0–10[%/100 nm]; medium red: gradient 10–25[%/100 nm]; very red: 25–40[%/100 nm]; outlyers: anything else.

| Object<br>Dyn. Type | $M_R$<br>Radius<br>[mag]/[km] | $B-V$<br>$\delta B-V$<br>[mag] | $V-R$<br>$\delta V-R$<br>[mag] | $R-I$<br>$\delta R-I$<br>[mag] | $J-H$<br>$\delta J-H$<br>[mag] | $H-K_s$<br>$\delta H-K_s$<br>[mag] | grad$(B-I)$<br>grad$(V-I)$<br>[%/100 nm] | grad(spectrum)<br>Spectral Type<br>[%/100 nm] |
|---|---|---|---|---|---|---|---|---|
| **1992QB1** | $6.82 \pm 0.06$ | 1.00 | 0.60 | 0.56 | — | — | $30 \pm 10$ | — |
| Cubewano | $120 \pm 3$ | 0.20 | 0.10 | 0.09 | — | — | $21 \pm 6$ | very red |
| **1993RO** | $8.56 \pm 0.08$ | — | 0.74 | 0.48 | — | — | — | — |
| Plutino | $54 \pm 2$ | | 0.11 | 0.11 | — | — | $25 \pm 7$ | very red |
| **1994EV3** | $7.08 \pm 0.15$ | — | 0.26 | 0.80 | — | — | — | — |
| Cubewano | $107 \pm 8$ | — | 0.20 | 0.20 | — | — | $16 \pm 9$ | blue outlyer |
| **1995HM5** | $22.39 \pm 0.29$(1) | — | — | — | 1.18 | — | — | — |
| Plutino | $67 \pm 10$(1) | — | — | — | 0.47 | — | — | outlyer?, peculiar $H-K$ |
| **1995SM55** | $4.20 \pm 0.03$ | 0.68 | 0.28 | 0.39 | — | — | $-1 \pm 1$ | $-12 \pm 5$ |
| Cubewano | $404 \pm 6$ | 0.06 | 0.04 | 0.04 | — | — | $-1 \pm 1$ | bluish |
| **1996RQ20** | $6.82 \pm 0.05$ | 0.89 | 0.68 | 0.58 | — | — | $30 \pm 8$ | — |
| Cubewano | $112 \pm 3$ | 0.14 | 0.09 | 0.09 | — | — | $27 \pm 7$ | very red |
| **1996TL66** | $5.30 \pm 0.06$ | 0.35 | 0.63 | 0.37 | — | — | $0 \pm 3$ | — |
| Scattered | $243 \pm 7$ | 0.09 | 0.08 | 0.09 | — | — | $13 \pm 4$ | neutral to slightly red |
| **1996TO66** | $4.36 \pm 0.03$ | 0.56 | 0.48 | 0.23 | — | — | $-2 \pm 2$ | $3 \pm 3$ |
| Cubewano | $375 \pm 5$ | 0.07 | 0.04 | 0.05 | — | — | $1 \pm 2$ | neutral to slightly red |
| **1996TP66** | $7.05 \pm 0.06$ | 1.03 | 0.58 | 0.66 | — | — | $36 \pm 6$ | — |
| Plutino | $109 \pm 3$ | 0.10 | 0.08 | 0.09 | — | — | $26 \pm 6$ | very red |
| **1997CQ29** | $6.86 \pm 0.08$ | — | 0.72 | 0.61 | 0.66 | — | — | $27 \pm 5$ |
| Cubewano | $109 \pm 4$ | — | 0.14 | 0.14 | 0.39 | — | $31 \pm 13$ | very red |
| **1997CS29(VLT)** | $4.76 \pm 0.04$ | 0.89 | 0.72 | 0.54 | 0.31 | 0.36 | $30 \pm 4$ | $27 \pm 3$ |
| Cubewano | $312 \pm 6$ | 0.08 | 0.06 | 0.05 | 0.16 | 0.23 | $27 \pm 4$ | very red |
| **1997CS29 (CA)** | $4.97 \pm 0.03$ | 1.03 | 0.78 | 0.54 | — | — | $50 \pm 6$ | — |
| as above | $283 \pm 4$ | 0.08 | 0.06 | 0.06 | — | — | $40 \pm 5$ | as above |
| **1998HK151** | $6.86 \pm 0.03$ | — | 0.45 | 0.42 | — | — | — | $7 \pm 3$ |
| Plutino | $118 \pm 2$ | — | 0.04 | 0.04 | — | — | $7 \pm 3$ | neutral to slightly red |
| **1998TF35** | $8.60 \pm 0.03$ | 1.02 | 0.71 | 0.57 | — | — | $38 \pm 8$ | — |
| Centaur | $53 \pm 1$ | 0.11 | 0.06 | 0.09 | – | — | $29 \pm 6$ | very red |
| **1998VG44** | $6.16 \pm 0.03$ | 0.93 | 0.61 | 0.77 | — | — | $39 \pm 5$ | — |
| Plutino | $163 \pm 2$ | 0.05 | 0.04 | 0.04 | — | — | $35 \pm 5$ | very red |
| **1998WH24** | $4.53 \pm 0.02$ | 0.83 | 0.64 | 0.39 | — | — | $16 \pm 2$ | — |
| Cubewano | $347 \pm 3$ | 0.06 | 0.04 | 0.04 | — | — | $15 \pm 3$ | medium red |
| **1998XY95** | $6.39 \pm 0.07$ | 0.93 | 0.65 | 0.77 | — | — | $41 \pm 16$ | — |
| Scattered | $147 \pm 5$ | 0.23 | 0.14 | 0.16 | — | — | $38 \pm 13$ | very red |
| **1999TC36** | $4.77 \pm 0.02$ | 0.96 | 0.70 | 0.58 | — | — | $35 \pm 2$ | — |
| Plutino | $310 \pm 3$ | 0.04 | 0.04 | 0.04 | — | — | $29 \pm 3$ | very red |
| **Sun** | | 0.67 | 0.36 | 0.33 | 0.29 | 0.06 | 0 | |

Notations: VLT = measured at VLT, CA = measured at Calar Alto.

Photometry – the measurement of the magnitude of the observed objects was made according to the same procedures used for the FORS1 data. Actually the procedures work much better here, because the background stars were dimmed by the median average.

The measurements of the standard stars followed the same procedure apart that the realignment was done to the stars themselves. By applying colour and air mass correction for La Silla the NTT/SOFI zero points were obtained. Since the emission of the sky in the infrared region is much larger than that in the visible, the greatest error contribution in the measured magnitude was the sky noise.

### 3.3. Spectroscopic data

**FORS1:** basic reduction steps – the raw exposures were first bias subtracted, flat field corrected and cosmic ray filtered. The bias frame was the median of several frames recorded at the beginning and the end of the night. The master flat field was computed as the median of several

exposures measured on the illuminated internal screen of FORS1, normalised to one. Since the sharpest intensity variations were in wavelength direction, a median filter of dimensions equal to 1 pixel in the $\lambda$-direction and 3 pixels along the slit was used to filter the cosmic rays. It was also checked that almost all and only cosmic rays were eliminated, by inspecting the difference image between unfiltered and filtered ones.

Wavelength solution and object signal extraction – by using HeAr spectra, the dispersion curve was obtained and the spectra were calibrated in wavelength. At the same time possible geometrical distorsions of the lines were also corrected. By integrating over the along-slit extension of the spectral profiles and subtracting the sky lines, one-dimensional spectra of the objects were obtained. For this operation particular care was necessary in order to use the minimum possible width of the spectrum for the extraction of the object signal, without loosing signal or introducing possible artificial colour, since the spectra were very weak and the sky contribution high.

Response and flux calibration – spectrophotometric standard star spectra, once corrected for air mass extinction, were used to derive the instrumental response curve. The response was used to obtain the flux calibrated target spectra. Finally, all spectra available for a single object were co-added and convolved with the instrumental point spread function (a Gaussian profile with $FWHM = 2.5$ nm).

Object reflectance – the reflectance curves of the TNOs were obtained by dividing the respective final spectra of an object by the catalogue solar spectrum, flux calibrated, and convolved with the same instrumental point spread function.

In the final spectra (both the flux calibrated and the reflectance ones) the major source of noise is produced by the sky emission lines, some of which amount to more than 10 times the signal of the objects.

## 4. Results

The filter photometry of the observed TNOs and Centaur as obtained from our images is given in Tables 2 and 3. Table 4 lists the absolute brightness $M_R$, the equivalent radius and the colours of the objects as derived from the data in Tables 2 and 3. It also lists the spectral gradients of the TNOs as obtained from the colours ($B-I$ and $V-I$) and from spectra (red, blue+red) and provides a type indication from both the orbit (Dyn. Type) and the photometric (Spectral Type) data.

The reflectivity spectra of the observed TNOs are shown in Fig. 1. Figure 2 shows their $V-I$ colours versus the absolute brightness in the $R$ passband. Colour-colour diagrams of the TNOs and Centaurs are given in Fig. 3. The reddening gradient statistics of the TNOs and Centaurs is displayed in Fig. 4. Figures 1 and 2 show results of our own observations only. Figures 3 and 4 show the results from the merged set of our data and the ones found in literature (see also Table 5).

The absolute magnitude $M_R$ of the object is derived from its $R$ filter brightness using the formula for asteroids (adopted by IAU Commission 20; Meeus 1998). For the phase correction factor $G$ a standardised value of 0.15 is applied. The error of $M_R$ is identical with the measurement uncertainty of the $R$ filter brightness. $M_R$ can be considered as a measure of the product "geometric cross-section $\times$ albedo of the object". The equivalent radius of the object is obtained applying the classical formula by Wyckhoff (1982) and assuming an albedo of 0.04. With one exception (1995HM5 for which we have near-IR data only) our absolute magnitude and equivalent radii refer to $R$ filter brightnesses of the objects.

The colour gradients grad$(C1-C2)$ indicate the reddening of the objects. For our data presented in Table 4 grad$(C1-C2)$ is derived from $B-I$ and $V-I$ colours. They are given in "percent per 100 nm" and can be calculated via formula (1):

$$\mathrm{grad}(C1-C2)=\frac{10^{0.4\times[(C1_{\mathrm{obj}}-C2_{\mathrm{obj}})-(C1_{\odot}-C2_{\odot})]}-1}{|\lambda_{C1}-\lambda_{C2}|}10^4 \quad (1)$$

where

$C1_{\mathrm{obj}}$, $C2_{\mathrm{obj}}$: the brightness of the TNO/Centaur in filters $C1$ and $C2$,

$C1_{\odot}$, $C2_{\odot}$: the filter brightness of the Sun,

$\lambda_{C1,C2}$: the central wavelength of the filters $C1$ and $C2$.

The corresponding spectral gradients can be measured directly from the reflectance spectra of the objects (using the "reference wavelength ranges" of 600–900 nm for the red spectra and 400–900 nm if blue and red spectra are available).

### 4.1. Reflectance spectra

The reflectance spectra of the 5 TNOs observed (see Fig. 1) are featureless, i.e. without indications for (neither emission nor absorption) spectral lines or bands intrinsic to the objects. The scatter in the red end of the spectra is due to incomplete subtraction of very bright skylines.

The spectral gradients are very constant over the measured wavelength ranges. However, marginal changes of the spectral slopes exist towards the red end of some spectra possibly indicating less steep reddening of the objects towards the near-IR region. Overall, the spectral gradients agree very well with the photometric ones for all measured objects except 1995SM55 for which the spectrum shows a negative gradient while the photometry gives neutral colours; see also Sect. 4.2.

### 4.2. Properties of individual objects

In this section we present short portraits of the individual TNOs/Centaur observed. Their characterisation is based upon our results and data published in literature. The objects are listed according to temporal order of designation.

1992QB1: the $M_R$ brightness of 7.00 mag corresponds to an equivalent radius of 110 km (albedo = 0.04),

**Table 5.** Average magnitudes and colours. The data presented in this table are calculated by averaging the results from the various publications as mentioned in the text. Column Class gives the dynamical class of the orbit of the objects: QB1 = Cubewano, Plut = Plutino, Scat = scattered disk object, Cent = Centaur. Column grad is the spectral gradient (%/100 nm) fitted over the available colour intervals per object. $\sigma$ gives the statistical error of the averaged colour and fitted spectral gradient values, respectively.

| Object | Class | $U-B\pm\sigma$ [mag] | $B-V\pm\sigma$ [mag ] | $V-R\pm\sigma$ [mag] | $R-I\pm\sigma$ [mag] | $V-J\pm\sigma$ [mag] | $J-H\pm\sigma$ [mag] | $H-K\pm\sigma$ [mag] | grad $\pm\sigma$ [%/100 nm] |
|---|---|---|---|---|---|---|---|---|---|
| 2060 Chiron | Cent | — | 0.679 ± 0.039 | 0.363 ± 0.027 | 0.354 ± 0.039 | 1.199 ± 0.110 | 0.290 ± 0.066 | 0.064 ± 0.080 | 0.8 ± 1.6 |
| Pho5145 | Cent | — | 1.307 ± 0.102 | 0.794 ± 0.032 | 0.822 ± 0.058 | 2.670 ± 0.054 | 0.375 ± 0.045 | −0.038 ± 0.044 | 52.5 ± 2.1 |
| 7066 Nessus | Cent | — | 1.090 ± 0.040 | 0.795 ± 0.043 | 0.690 ± 0.040 | — | 0.319 ± 0.292 | −0.120 ± 0.424 | 44.6 ± 2.1 |
| 8405 Asbolus | Cent | — | 0.750 ± 0.040 | 0.522 ± 0.072 | 0.525 ± 0.049 | 1.720 ± 0.177 | 0.306 ± 0.150 | 0.097 ± 0.279 | 15.7 ± 3.1 |
| 10199 Chariklo | Cent | — | 0.770 ± 0.050 | 0.470 ± 0.034 | 0.546 ± 0.031 | — | 0.408 ± 0.047 | 0.086 ± 0.050 | 13.4 ± 1.7 |
| 10370 Hylomene | Cent | — | 0.670 ± 0.071 | 0.474 ± 0.060 | — | — | — | — | 11.4 ± 6.2 |
| 1992QB1 | QB1 | — | 0.813 ± 0.142 | 0.719 ± 0.093 | 0.637 ± 0.212 | — | — | — | 36.8 ± 6.6 |
| 1993FW | QB1 | — | 0.932 ± 0.089 | 0.517 ± 0.101 | 0.431 ± 0.127 | — | — | — | 12.2 ± 5.5 |
| 1993RO | Plut | — | 0.933 ± 0.162 | 0.576 ± 0.128 | 0.515 ± 0.192 | — | — | — | 19.4 ± 7.5 |
| 1993SB | Plut | — | 0.820 ± 0.030 | 0.462 ± 0.068 | — | — | — | — | 10.1 ± 7.1 |
| 1993SC | Plut | — | 1.008 ± 0.108 | 0.659 ± 0.062 | 0.736 ± 0.082 | 2.434 ± 0.155 | 0.400 ± 0.203 | −0.040 ± 0.197 | 35.3 ± 3.5 |
| 1994ES2 | QB1 | — | 0.710 ± 0.150 | 0.940 ± 0.150 | 0.970 ± 0.150 | — | — | — | 80.4 ± 7.4 |
| 1994EV3 | QB1 | — | 1.500 ± 0.150 | 0.511 ± 0.128 | 0.800 ± 0.199 | — | — | — | 25.6 ± 7.6 |
| 1994JQ1 | QB1 | — | — | 0.945 ± 0.097 | — | — | — | — | — |
| 1994JR1 | Plut | — | 1.010 ± 0.180 | 0.656 ± 0.115 | 0.520 ± 0.120 | — | — | — | 24.8 ± 5.8 |
| 1994JS | QB1 | — | — | 0.850 ± 0.070 | — | — | — | — | — |
| 1994JV | QB1 | — | — | 0.771 ± 0.091 | 0.563 ± 0.133 | 1.333 ± 0.188 | — | — | 37.0 ± 5.3 |
| 1994TA | Cent | — | 1.240 ± 0.060 | 0.680 ± 0.030 | — | — | — | — | 35.2 ± 3.2 |
| 1994TB | Plut | — | 1.043 ± 0.167 | 0.709 ± 0.088 | 0.716 ± 0.148 | 2.485 ± 0.152 | — | — | 38.7 ± 5.5 |
| 1994VK8 | QB1 | — | 1.010 ± 0.060 | 0.659 ± 0.061 | — | — | — | — | 32.6 ± 6.3 |
| 1995DA2 | QB1 | — | — | 0.550 ± 0.110 | 0.500 ± 0.160 | — | — | — | 16.9 ± 6.4 |
| 1995DC2 | QB1 | — | — | 0.770 ± 0.160 | 0.580 ± 0.160 | — | — | — | 36.5 ± 7.9 |
| 1995HM5 | Plut | — | 0.649 ± 0.102 | 0.463 ± 0.096 | 0.370 ± 0.108 | — | 1.180 ± 0.470 | — | 6.8 ± 4.9 |
| 1995QY9 | Plut | — | 0.696 ± 0.121 | 0.520 ± 0.093 | 0.400 ± 0.060 | 2.027 ± 0.201 | — | — | 10.6 ± 4.0 |
| 1995QZ9 | Plut | — | 0.880 ± 0.040 | 0.515 ± 0.050 | — | — | — | — | 15.7 ± 5.2 |
| 1995SM55 | QB1 | — | 0.680 ± 0.058 | 0.357 ± 0.098 | 0.390 ± 0.042 | — | — | — | 1.8 ± 3.9 |
| 1995WY2 | QB1 | — | 0.990 ± 0.150 | 0.680 ± 0.150 | 0.430 ± 0.150 | — | — | — | 22.6 ± 7.4 |
| 1996RQ20 | QB1 | — | 0.890 ± 0.144 | 0.523 ± 0.133 | 0.580 ± 0.094 | — | — | — | 18.1 ± 5.9 |
| 1996RR20 | Plut | — | 1.160 ± 0.040 | 0.710 ± 0.030 | — | — | — | — | 39.0 ± 3.2 |
| 1996SZ4 | Plut | — | 0.830 ± 0.030 | 0.520 ± 0.020 | — | — | — | — | 16.3 ± 2.2 |
| 1996TK66 | QB1 | — | 0.990 ± 0.020 | 0.630 ± 0.020 | — | — | — | — | 29.0 ± 2.2 |
| 1996TL66 | Scat | 0.970 ± 0.190 | 0.652 ± 0.082 | 0.344 ± 0.066 | 0.456 ± 0.090 | 1.452 ± 0.114 | 0.350 ± 0.117 | −0.040 ± 0.112 | 5.2 ± 3.5 |
| 1996TO66 | QB1 | 1.000 ± 0.120 | 0.641 ± 0.066 | 0.384 ± 0.048 | 0.356 ± 0.063 | 0.997 ± 0.101 | −0.210 ± 0.170 | 0.810 ± 0.158 | 5.2 ± 2.5 |
| 1996TP66 | QB1 | — | 0.904 ± 0.121 | 0.636 ± 0.083 | 0.668 ± 0.088 | 2.309 ± 0.060 | 0.170 ± 0.078 | 0.020 ± 0.092 | 30.2 ± 4.2 |
| 1996TQ66 | Plut | — | 1.160 ± 0.100 | 0.645 ± 0.080 | — | 2.435 ± 0.128 | — | — | 30.8 ± 8.2 |
| 1996TS66 | QB1 | — | 0.974 ± 0.083 | 0.605 ± 0.145 | 0.670 ± 0.120 | 1.824 ± 0.178 | 0.650 ± 0.071 | — | 28.0 ± 6.7 |
| 1997CQ29 | QB1 | — | 0.990 ± 0.124 | 0.754 ± 0.127 | 0.616 ± 0.113 | — | — | — | 36.9 ± 6.0 |
| 1997CR29 | QB1 | — | 0.790 ± 0.100 | 0.470 ± 0.080 | 0.680 ± 0.120 | — | — | — | 17.8 ± 4.7 |
| 1997CS29 | QB1 | — | 1.016 ± 0.083 | 0.678 ± 0.054 | 0.571 ± 0.064 | 2.073 ± 0.134 | 0.310 ± 0.156 | 0.360 ± 0.233 | 28.9 ± 2.9 |
| 1997CT29 | QB1 | — | — | 0.744 ± 0.090 | — | — | — | — | — |
| 1997CU29 | QB1 | — | 1.172 ± 0.174 | 0.640 ± 0.048 | 0.651 ± 0.108 | — | — | — | 29.8 ± 3.4 |
| 1997QH4 | QB1 | — | 1.010 ± 0.070 | 0.670 ± 0.050 | — | — | — | — | 33.9 ± 5.2 |
| 1997QJ4 | Plut | — | — | 0.460 ± 0.086 | — | — | — | — | — |
| 1997SZ10 | QB1 | — | 1.140 ± 0.080 | 0.650 ± 0.030 | — | — | — | — | 31.4 ± 3.2 |
| 1998FS144 | QB1 | — | 0.910 ± 0.076 | 0.560 ± 0.067 | — | — | — | — | 20.8 ± 6.9 |
| 1998HK151 | Plut | — | 0.510 ± 0.090 | 0.469 ± 0.065 | 0.398 ± 0.073 | — | — | — | 8.0 ± 3.4 |
| 1998KG62 | QB1 | — | 1.000 ± 0.060 | 0.561 ± 0.074 | 0.640 ± 0.040 | — | — | — | 23.4 ± 3.1 |
| 1998QM107 | Cent | — | 0.730 ± 0.060 | 0.520 ± 0.030 | — | — | — | — | 16.3 ± 3.2 |
| 1998SG35 | Cent | — | 0.890 ± 0.110 | 0.430 ± 0.080 | 0.590 ± 0.080 | — | — | — | 12.5 ± 3.9 |
| 1998SM165 | QB1 | — | 1.010 ± 0.100 | 0.750 ± 0.070 | — | — | — | — | 44.4 ± 7.2 |
| 1998SN165 | QB1 | — | 0.820 ± 0.080 | 0.470 ± 0.161 | 0.510 ± 0.080 | — | — | — | 12.0 ± 6.6 |
| 1998TF35 | Cent | — | 1.020 ± 0.108 | 0.710 ± 0.057 | 0.573 ± 0.095 | — | — | — | 32.6 ± 3.5 |
| 1998UR43 | Plut | — | — | 0.616 ± 0.107 | — | — | — | — | — |
| 1998VG44 | Plut | — | 0.951 ± 0.055 | 0.567 ± 0.056 | 0.668 ± 0.116 | — | — | — | 24.1 ± 3.8 |
| 1998WH24 | QB1 | — | 0.907 ± 0.058 | 0.607 ± 0.043 | 0.536 ± 0.158 | 1.771 ± 0.076 | — | — | 24.4 ± 3.7 |
| 1998WV24 | Plut | — | 0.770 ± 0.010 | 0.500 ± 0.030 | — | — | — | — | 14.1 ± 3.2 |
| 1998WX24 | QB1 | — | 1.090 ± 0.050 | 0.700 ± 0.050 | — | — | — | — | 37.7 ± 5.2 |
| 1998XY95 | Scat | — | 0.939 ± 0.238 | 0.645 ± 0.140 | 0.772 ± 0.153 | — | — | — | 36.2 ± 7.1 |
| 1999OX3 | Scat | — | 1.072 ± 0.117 | 0.692 ± 0.055 | — | — | — | — | 36.8 ± 5.7 |
| 1999OY3 | QB1 | — | 0.710 ± 0.010 | 0.370 ± 0.020 | — | — | — | — | 1.0 ± 2.2 |
| 1999RY215 | QB1 | — | 0.800 ± 0.100 | — | 0.780 ± 0.080 | — | — | — | — |
| 1999RZ253 | QB1 | — | 0.820 ± 0.170 | — | — | — | — | — | — |
| 1999TC36 | Plut | — | 0.965 ± 0.056 | 0.685 ± 0.048 | 0.622 ± 0.085 | — | — | — | 32.5 ± 3.1 |
| 1999TD10 | Scat | — | 0.770 ± 0.050 | 0.470 ± 0.050 | — | — | — | — | 10.9 ± 5.2 |
| 1999TR11 | Plut | — | 1.020 ± 0.080 | 0.750 ± 0.070 | — | — | — | — | 44.4 ± 7.2 |
| 1999UG5 | Cent | — | 0.921 ± 0.157 | 0.617 ± 0.071 | 0.621 ± 0.045 | — | — | — | 26.4 ± 3.0 |
| 2000EB173 | Plut | — | 0.964 ± 0.053 | 0.550 ± 0.097 | 0.633 ± 0.089 | — | — | — | 22.2 ± 4.6 |
| 2000PE30 | QB1 | — | 0.710 ± 0.050 | 0.380 ± 0.040 | 0.450 ± 0.040 | — | — | — | 4.7 ± 2.0 |
| 2000WR106 | QB1 | — | 1.017 ± 0.071 | 0.711 ± 0.071 | 0.730 ± 0.071 | — | — | — | 39.6 ± 3.5 |
| Sun | | 0.2 | 0.67 | 0.36 | 0.33 | 1.08 | 0.29 | 0.06 | 0 |

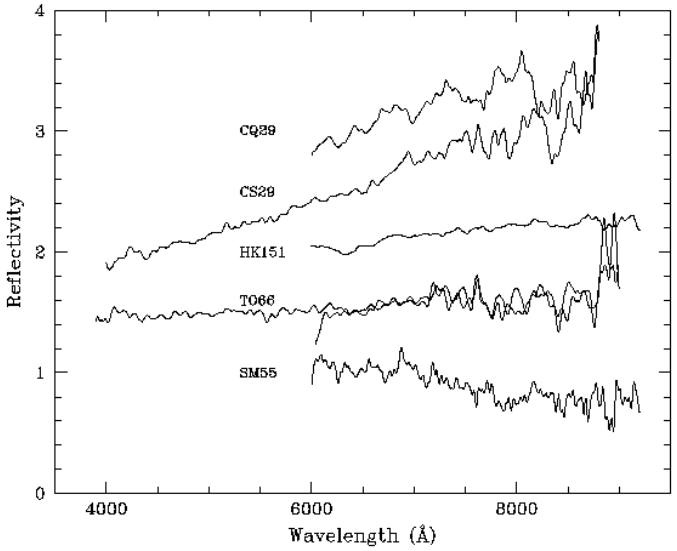


**Fig. 1.** Reflectance spectra of 5 TNOs. The spectra were taken with two different settings for the wavelength coverage, see Table 1. The scatter beyond 750 nm is due to incomplete subtraction of strong skylines. The reflectance spectra of the individual objects are offset by an arbitrary value for better display. For 1996TO66 the "red+blue" and the "red only" spectra (see note (1) in Table 2) are shown: the good overlap of both spectra proves that first order contamination in the red is neligible.

i.e. 1992QB1 may be of medium size. According to our *BVRI* colour measurements this TNO is a typical red object (gradient of about 30%/100 nm). While our *VRI* colours are in good agreement (though more accurate) with those of Luu & Jewitt (1996) the $B$ magnitude differs by 0.35 mag (ours being redder). This deviating $B$ brightness explains why 1992QB1 was previously considered an outlyer in the $V-R$ versus $B-V$ diagram. According to our data 1992QB1 falls pretty much in the centre of the red cloud of objects in both colour-colour diagrams (see Fig. 3). One can speculate whether a change of the physical properties of the TNO or problems with the earlier $B$ filter measurements (our favoured interpretation) are responsible for the colour change in $B-V$. Neither a visible spectrum nor near-IR data of 1992QB1 are available so far.

1993RO: this TNO is fainter and most likely smaller than 1992QB1 (see Table 4). The *VRI* colours are red ($V-I$ spectral slope of 25%/100 nm). The published *VRI* data (Luu & Jewitt 1996) are in agreement with ours, while their $B-V$ index is even steeper. Visible spectroscopy and *JHK* data of this object are still missing.

1994EV3: this medium bright TNO (see Table 4) is a puzzling object. It appears to be very red according to the $B-V$ and $R-I$ indices measured by Luu & Jewitt (1996) and in our own data of 1999. Contrary to this, 1994EV3 has only slightly reddish (Luu & Jewitt 1996) to slightly bluish (ours) $V-R$ colours. Unfortunately, no further observations (visible and near-IR) of this exceptional TNO are reported.

1995HM5: we have *JH* magnitudes of this object only. Taking the $M_J$ value of 7.30 mag, this object would be one of the smaller TNOs known so far (about 65 km equivalent radius for albedo 0.04). Our $J$ filter radius is not too different from the one (about 80 km) obtained in the visible wavelength range (Tegler & Romanishin 1998). The published *BVRI* colours (Tegler & Romanishin 1998; Barucci et al. 2000) assign an almost neutral colour gradient to 1995HM5. Our $J-H$ value of 1.18 mag is, however, very red, but also very uncertain. If confirmed, it would make 1995HM5 a rather peculiar object (neutral in the visible, very red in near-IR) among the TNOs. Only colours of the object are measured so far.

1995SM55: this large (i.e. bright) TNO has *VRI* and a red spectrum measured. Both observations indicate that 1995SM55 is a neutral to slightly bluish object. The spectrum (see Fig. 1) displays a somewhat bluer gradient although with a trend to flatten off beyond 800 nm. This object had no colours or spectra published so far.

1996RQ20: another medium-sized object ($M_R$ = 6.99 mag, equivalent radius = 110 km for 0.04 albedo). From its *BVRI* colours (gradient of about 30%/100 nm) this object appears to be a reddish TNO similar to 1997CS29. The only $V-R$ measurement available from literature (0.44 mag; Tegler & Romanishin 1998) would classify this TNO as neutral, which is in clear disagreement with our data. No spectrum nor near-IR photometry of 1996RQ20 are measured so far.

1996TL66: 1996TL66 is among the group of larger (brighter) TNOs. From the 3 colours measured only the $R-I$ value in our data is in agreement with the ones published elsewhere (see Barucci et al. 1999a for a summary). Our $B-V$ and $V-R$ for 1996TL66 deviates from those found by other groups. However, our $B-R$ colour is very close to the ones calculated from the table of Barucci et al. This may indicate that the $V$ filter brightness in our data may be wrong although we can't find any obvious reason from the analysis of the data. In any case the $B-V$ and $V-R$ gradient which follows from our measurements seems to be against our experience that spectral gradients of TNOs in the visible wavelength range seem to be "straight" (see also Sect. 4.1). The visible spectrophotometry and the near-IR spectroscopy published by Luu & Jewitt (1998) shows a flat featureless spectrum with neutral colours from $V$ to $K$ band.

1996TO66: the $M_R$ brightness of 4.53 mag is almost exactly identical with the one found from earlier photometry (Hainaut et al. 2000a). It corresponds to an equivalent radius (albedo = 0.04) of 345 km which would make this objects one of the largest TNOs known so far. Our new data – colours and spectra – classifies 1996TO66 to be a neutral object. The two available spectra of 1999 confirm the quasi-simultaneous photometric colours. A close comparison with the 1997 spectrum (Hainaut et al. 2000a) shows marginal differences between the 1997 red (beyond 750 nm) and 1999 blue-to-red gradients. The photometric colours of Dec. 1999

agree well with the ones measured earlier (Jewitt & Luu 1998; Barucci et al. 1999b; Hainaut et al. 2000a). This implies that the change in the amplitude of the rotation light curve of this object observed between 1997, 1998 and 1999 had no or very little impact on the object colours and spectrum; (for a new study of the light curve of this TNO see Sekiguchi et al. 2001). 1996TO66 is a representative of the neutral colour TNOs and it is considered the most interesting TNO observed so far: water absorption in $H$ and $K$ band (Brown et al. 1999), light curve changes (Hainaut et al. 2000a).

1996TP66: this rather bright and most likely large TNO is also a very red object (gradient of about 35%/100 nm, i.e. redder than 1997CS29). Our *BVRI* colours are in good agreement with the ones of Tegler & Romanishin (1998), Jewitt & Luu (1998) and Barucci et al. (1999b). In the near-IR its spectral slope gets flat with $H - K$ being of solar value (Noll et al. 2000).

1997CQ29: with 110 km equivalent radius ($M_R$ = 7.05 mag) this TNO may be a medium size body in the Edgeworth-Kuiper Belt. The variability in the $V$ filter brightness (0.38 mag, see Tables 2 and 3) is due to the body's rotation and may indicate an aspherical shape (axis ratio >1.45) and/or albedo variations (factor ∼2) on its surface. Our visible data indicate that this object may be very similar to 1997CS29: a typical red TNO (constant gradient of about 30%/100 nm from about 500 to 900 nm). The $V - J$ and $J - H$ colours appear to be larger as compared to 1997CS29 which may be due to the large uncertainty in our photometry and/or due to rotational variability over the long near-IR integration times. Our *VRI* photometry agrees with that of Tegler & Romanishin (1998), the $V - J$ colour differs – by about 0.1 mag – from that of Davies et al. (2000) – possibly because of the rotation light curve of the object.

1997CS29: this object appears to be a large TNO ($M_R$ of about 4.85 mag or 290 km equivalent radius) with a red spectrum and red colours in the optical wavelength range. The featureless visible spectrum (see Fig. 1) displays a constant gradient of 27%/100 nm from 400 to 900 nm with only marginal indications of a somewhat smaller slope beyond 800 nm. The VLT *BVRI* colours agree with the spectrum. However, they disagree with the $B - V$ colour published by Tegler & Romanishin 1998 (ours: 0.89 mag, Tegler & Romanishin: 1.17 mag); our (quasi-simultaneous) spectrum and photometry does not support such a strong reddening in the blue wavelength range as indicated by the $B - V$ value of Tegler & Romanishin. The Calar Alto results for *BVRI* lie in between the ones from the VLT and Tegler & Romanishin. They agree with the VLT ones for adjacent filter colours within the error bars, but they have a trend to a slightly redder gradient such that the $B - I$ and $V - I$ colours clearly deviate from the VLT ones. From our Calar Alto $R$ band monitoring of this object over 3 nights (unpublished) we conclude that 1997CS29 is a slow rotator with a rotation period clearly longer than one day. Therefore, the discrepancy between the three data sets is either intrinsic to this object or due to inconsistencies in the data reduction of the various groups. In the near-IR filters $JHK_s$ the colour reddening becomes smaller with a clear trend to level off towards the long wavelength end. 1997CS29 appears to be a typical representative of the red TNO population ($B - I$ spectral gradient agrees with peak value in the respective population statistics; see Sect. 5).

1998HK151: this medium-sized/bright object ($M_R$ = 6.87 mag, equivalent radius of 120 km for albedo 0.04) belongs to the group of TNOs with neutral to only very slightly red colours. The spectral gradient of 7%/100 nm obtained from our *VRI* colours is in exact agreement with the one measured in our spectrum. This spectrum is the best one we have in terms of $S/N$ (we had 0.4″ seeing during the 1 hour integration time), but it is still not good enough to search with success for absorption bands in the red part of the spectrum. However, a small turn-over to a flatter slope is found beyond about 800 nm. The object was measured with almost constant $V$ filter brightness in two subsequent nights. No comparison data are available in literature.

1998TF35: the only Centaur in our sample is of about 50 km size (according to its absolute brightness in $R$). It is a red object more like the typical red TNOs, but not as red as the two other red Centaurs, 5145 Nessus and 7066 Pholus (Barucci et al. 1999a and references therein). No comparison data are available in literature.

1998VG44, 1998XY95, 1999TC36: these TNOs, although different in their absolute magnitude and thus possibly in size, have very similar *BVRI* colours. They all belong to the group of typical red TNOs with colour gradients of 30–40%/100 nm. Our measurements for 1998VG44 are in agreement with the ones of Doressoundiram et al. (2001) except for $R - I$ for which the deviation is slightly higher (0.05 mag) than compatible with the claimed photometric errors. near-IR data of all three objects are not available.

1998WH24 one of the largest TNOs measured so far ($M_R$ = 4.68 mag, equivalent radius of about 350 km for albedo 0.04) shows intermediate red colours. The $I$ band brightness would indicate an unusual $R - I$ gradient, but it is most likely contaminated since the photometry was done in the immediate neighbourhood of a bright star (the given uncertainty is a formal error). This is also apparent when comparing our data with those of Barucci et al. (2000): while $B - V$ and $V - R$ agree within the error bars, $R - I$ does not. No spectra and near-IR data of this TNO are published so far.

In summary: in our ESO and Calar Alto observations from 1998 to 2000 we could identify

- 4 neutral, slightly bluish or slightly reddish TNOs (1995SM55, 1996TL66, 1996TO66, 1998HK151);
- 1 intermediate red TNO (1998WH24);
- 9 red TNOs (1992QB1, 1993RO, 1996RQ20, 1996TP66, 1997CQ29, 1997CS29, 1998VG44, 1998XY95, 1999TC36);
- 1 red Centaur (1998TF35);
- 2 TNOs appear as outlyers (1994EV3, 1995HM5).

With a few exceptions, our colour values confirm the ones reported for the respective objects in literature. In the few cases for which spectra of TNOs are available, the spectroscopic colour gradients are in good agreement with the ones determined from (quasi-simultaneous) photometric data.

## 5. Photometric characterisation of TNOs – comparison between TNOs and Centaurs

For the group characterisation of objects we apply colour-magnitude (see Fig. 2) and colour-colour diagrams (see Fig. 3) as well as the statistics of colour gradients (see Fig. 4). For the two latter plots we distinguish between dynamical classes: Centaurs (TNOs migrating inward, i.e. with orbits between Jupiter and Neptune), Plutinos (TNOs in Pluto-like orbits, i.e. in 2/3 resonance with Neptune), Cubewanos (TNOs in the main Kuiper Belt outside of the 2/3 resonance with Neptune), scattered disk objects (TNOs scattered into highly excentric orbits).

The colour-magnitude diagram uses only our own measurements of TNOs, while the colour-colour plots and the colour gradient statistics are based on a compilation which merges the results of our measurements with the table of object colours as published by Barucci et al. (1999b), supplemented by those of Barucci et al. (2000), Davies et al. (2000), Tegler & Romanishin (2000), Noll et al. (2000) and Doressoundiram et al. (2001). For each object for which quasi-simultaneous colours (i.e. free of lightcurve variability) are measured, the weighted mean value and its error are calculated. The weight factors are the errors of the individual colour data. The colour gradients are determined from the *BVRI* colour data in Table 5 by a linear regression fit over all individual colour gradients of a single object. A minimum of at least two colours per object must be available.

Table 5 lists the merged new table of mean broadband colours and spectral gradients per TNO (Plutinos, Cubewanos and scattered disk objects) and Centaur. The list contains in total 69 objects: 35 Cubewanos, 19 Plutinos, 4 scattered disk objects and 11 Centaurs. From the table 63 objects are used for the colour-colour plots shown in Fig. 3, and 62 for the colour gradient statistics shown in Fig. 4.

The low number of scattered disk objects and Centaurs with photometry measured, makes statistical conclusions on group properties very difficult. At best first trends can be derived. Also, for all dynamical classes the near-IR range is not yet covered by a large enough set of measured

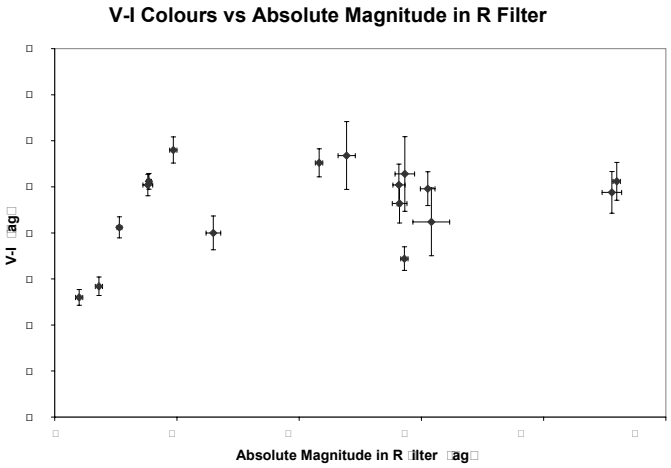


**Fig. 2.** Colour–absolute magnitude diagram of TNOs and Centaurs. The figure plots the $V-I$ colour of our own TNO & Centaur measurements versus the absolute magnitude as derived from the $R$ filter brightness of the objects. The plot includes 16 TNO and 1 Centaur measurements.

objects such that for the time being we will not include it in our discussion below.

**Colour-magnitude diagram**: this diagram (see Fig. 2) plots the $V-I$ colour versus the absolute magnitude $M_R$ of the objects in the $R$ band filter (see Table 4). Over the whole range of absolute magnitudes measured our data show no conclusive correlation between $M_R$ and the $V-I$ colours of the objects. At best – however based on only 6 data points – one could hypothesise a linear trend between $M_R$ and $V-I$ for the brightest TNOs (brighter than $M_R = 5$ mag). The absence of a clear relationship between $M_R$ and $V-I$ in Fig. 2 is in contrast with the results published by Jewitt & Luu (1998) and Davies et al. (2000). Both groups found a strong correlation between $M_V$ and $V-J$ using a sample of only 5 selected TNOs with high-quality measurements. Davies et al., however, cannot confirm this correlation using a larger sample of 14 TNOs. Our sample also suggests that the colour dispersion does not depend on $M_R$, i.e. on the product between cross-section (or size) and albedo of the object. Such a correlation is predicted from theoretical simulations of collision resurfacing of the objects (Luu & Jewitt 1996). However, a larger statistical sample needs to be analysed to confirm or disprove this suggestion.

**Colour-colour diagrams**: three colour-colour plots are presented using the merged data set of Table 5: $V-R$ versus $B-V$, $R-I$ versus $B-V$, and $R-I$ versus $V-R$ (Fig. 3).

*General trends:* the well known reddening trends of the TNO and Centaur populations are clearly visible in the plots. The colours range from about solar ones to about 1.2 mag in $B-V$ and 0.8 mag in $V-R$ and $R-I$. The colour ranges are about the same for the 4 dynamical object classes (Cubewanos, Plutinos, scattered disk objects, Centaurs). In the $V-R$ vs. $B-V$ plot the colour distribution of the objects follows nicely the line of increased reddening. However, there seem to be a trend of smaller

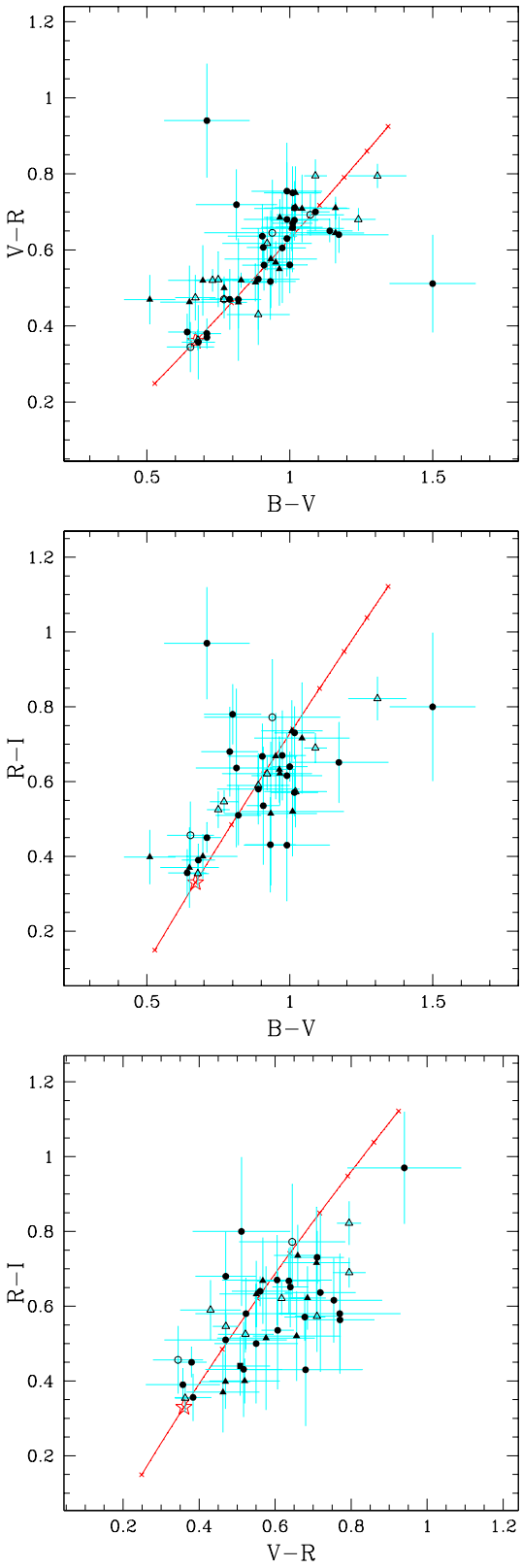


**Fig. 3.** Colour–colour diagrams of TNOs and Centaurs. Top: $V-R$ versus $B-V$. Middle: $R-I$ versus $B-V$. Bottom: $R-I$ versus $R-V$. The symbols are: filled circles = Cubewanos, filled triangles = Plutinos, open circles = scattered disk objects, open triangles = Centaurs. The solar colours are indicated by the open star symbol. For the plots the data from Table 5 are used as input. The lines indicates the direction of increased reddening from −10 to 90%/100 nm.

reddening in the $R-I$ vs. $V-R$ plot since the measured objects "fall" below the line of constant reddening towards the redder end of the colour distribution. This effect indicates slope changes towards the near-IR as noticed in the visible spectra of some of the objects (see Sect. 4.1). The deviations seems to be pronounced for the red population, but is widely absent for the neutral objects.

It is noteworthy that the TNOs of solar-type $B-V$ colours have also neutral $V-R$ and $R-I$ colours. The red $B-V$ cloud objects are also red in $V-R$ and $R-I$. This confirms the conclusion from our spectroscopy measurements that usually no sudden and significant changes of the spectral slope are seen in optical spectra of TNOs (see also Sect. 4.1).

*Outlyers:* there are a few exceptions from the general trends: 1994ES2 and 1994EV3, two Cubewanos that appear to be outlyers in their colours. According to their colours they should exhibit interesting spectra in the visible range; however, up to now no spectra of these TNOs are published. The 5145 Pholus is at the very red end of the colour distribution which makes it to the reddest Centaur known so far. For more details on these objects see Sect. 4.2.

*TNOs (Cubewanos, Plutinos and scattered disk objects)*: in the presented version the colour-colour plots of Fig. 3 do not show a clear bimodal distribution of TNOs (separated mostly in $B-V$ with a gap between $B-V$ of 0.7 to 0.9 mag) as described Tegler & Romanishin (1998). At best a certain clustering of the Cubewanos towards the red end of the colour distribution may be noteworthy while the two other dynamical classes – Plutinos and scattered disk objects – do not (yet) show any clear trends in the plots of Fig. 3. However, for both classes the number of objects measured is still small.

The bimodal distributions in the $V-R$ vs. $B-V$ plots reported earlier may be a selection effect due to the small number of objects measured. However, even with the much larger data set available now a two-dimensional Kolmogorov-Smirnow statistics analysis of the available colour data (Hainaut, priv. communication) concludes that the observed colour distribution (this includes also $B-V$ vs. $V-R$) is compatible with both a single continuous as well as with a double peak colour population of TNOs.

*Centaurs*: the measured Centaurs – although low in number – seem to populate the neutral and the red end of the colour distributions with only a single object (1999UG5) inbetween. 3 red Centaurs (5145 Pholus, 7066 Nessus and 1994TA) are placed at the upper end and beyond the red TNO cloud in the $B-V$ vs. $V-R$ diagram (see Fig. 3).

**Colour gradient statistics**: Table 5 lists also the colour gradients (or reddening) of the TNO and Centaurs as calculated from the colours of the same table. For the colour gradient statistics the number of objects per gradient interval is counted. The gradient intervals are set in steps of 10%/100 nm over the total gradient interval measured (which was −10 to 90%/100 nm). The

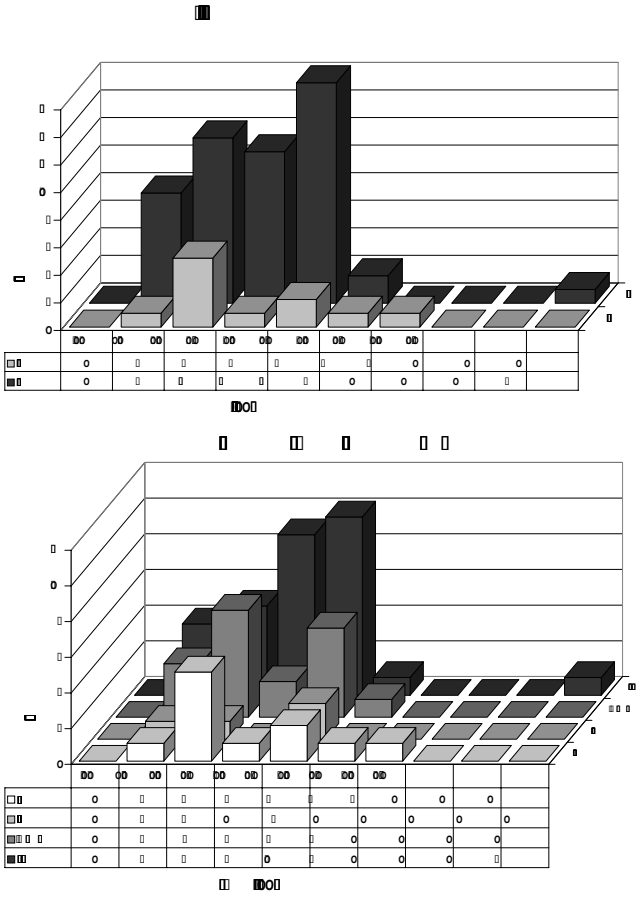

**Fig. 4.** Reddening gradient statistics of TNOs and Centaurs. Upper panel: all TNOs and Centaurs. Lower panel: dynamical classes: Cubewanos, Plutinos, scattered disk objects, Centaurs. The reddening of the objects (in %/100 nm) as compared to the Sun is calculated according to Eq. (1) and the number of objects ($Y$ axis) per reddening interval ($X$ axis) is counted.

chosen step width is approximately twice the average standard deviation of the majority of the individual gradient values. Although of arbitrary nature, this selection grid may somehow represent groups of objects with distinct differences in surface reddening. The gradient statistics obtained are presented in Fig. 4. One plot shows the statistics for the 4 dynamical classes Cubewanos, Plutinos, scattered disk objects and Centaurs individually, the other one compares the distributions of all TNOs (Cubewanos + Plutinos + scatterd disk objects) and Centaurs.

For TNOs – Cubewanos, Plutinos, scattered disk objects – the gradient statistics suggests the following conclusions:

- all TNOs: the majority of TNOs has reddening between 0 and 50%/100 nm; only one object (1994EV3) has a much steeper gradient;
- all TNOs: the distribution maximum falls between 20–40%/100 nm;
- Cubewanos: the colour gradient distribution increases systematically from 0 to the maximum between 30–40%/100 nm;
- Plutinos and scattered disk objects: their colour gradient statistics seem to have a double-peaked distribution.

For Centaurs we conclude from the colour gradient plots:

- the Centaurs show up in two separate reddening ranges: the majority (in total 6) falls in the reddening interval between 0–20%/100 nm, a minority has gradients of more than 30%/100 nm;
- the Centaurs of neutral colour tend to be "clustered", while the red objects spread over a wider gradient range.

In particular for the scattered disk objects and Centaurs – maybe even for the Plutinos – the number of objects in this analysis is still very small. Therefore, any conclusion on class properties of the visible photometry is still uncertain and needs confirmation by new and more observations.

The gradient statistics suggests a diversity in the predominant reddening between the 4 dynamical classes: the Cubewanos have a single peak distribution with a typical reddening of 20–40%/100 nm, while the 3 other classes resemble more a double peak distribution with a deficiency of objects in the reddening range of 20–30%/100 nm. At least for the Centaurs that are considered to be sunward scattered TNOs (Levison 2001) – but maybe also for the Plutinos and scattered disk objects – one can speculate that they may have undergone a colour change as compared to the TNOs in the classical Edgeworth-Kuiper-Belt.

The colour palette seen in objects of the outer solar system is usually attributed to the combined action of three effects:

1. High-energy radiation which could turn the ice-carbon mixture on the surface into complex hydrocarbon compounds of reddish colour. According to Shul'man (1972) the time scale for in-situ growth of an irradiated mantle (of several 10 cm thickness) is of the order of $10^7$ to $10^9$ years. Thin mantles grow faster which may imply that colour changes due to irradiation reddening may happen on time scales of a few million years;
2. Fresh ices from below the surface can be excavated by impacts of other objects. The ices from the crater area can be distributed over a wide surface range. Assuming that a major part of the surface is covered by fresh cratering deposits, the neutral surface colours may be explained. As demonstrated by Luu & Jewitt (1996), impact resurfacing – in combination with the high-energy radiation reddening – can produce any colour value observed in TNOs and Centaurs, depending on the collision rate or in other words the size distribution of the objects. The latter also defines the typical time scales for the impacts with significant resurfacing potential. Luu & Jewitt confirm the typical collision time scales of $10^6$ to $10^7$ years for the Edgeworth-Kuiper Belt region, first published by Stern (1995);

3. Intrinsic activity like in comets could produce a coma of volatile gases ($N_2$, CO like in the atmosphere of Pluto) around TNOs and Centaurs that can recondense (at least in parts) back onto the surface, thus forming a fresh ice layer. This scenario is proposed by Hainaut et al. (2000a) to explain the light curve change observed in 1996TO66. Although the surface temperature of the TNOs is very low (40–50 K) and only $N_2$ as well as CO and $CH_4$ ices may be able to sublimate on a very low level, atmospheric frost would have the same effect as impact resurfacing, i.e. producing neutral colours of the objects' surfaces. At present, no estimations of time scales for resurfacing by intrinsic activity are available. Obviously, the process of ice recondensing on the surface must be fast, if it shall explain the 1996TO66 case.

**Interpretation of the spectral diversities in TNOs and Centaurs:** Centaurs orbit the Sun at distances where collisions with other Solar System bodies are less likely (since the space between the major planets doesn't seem to be very populated with minor bodies). On the other side, since they get closer to the Sun, internal activity may be triggered more frequently and stronger due to more efficient solar heating of the surface layers. Therefore, cometary activity like that observed in the Centaur 2060 Chiron may cause resurfacing of Centaurs with freshly condensed frost and may account for the neutral to slightly reddish objects observed. If the intrinsic activity is not triggered (for instance due to strong crust formation on the surface), very red colours could develop with time due to high-energy radiation. Hence, a bimodal colour gradient distribution with very bluish and very red objects only – as seen in Figs. 3 and 4 – may result among the Centaurs. Although one could speculate that the closer the perihelion to the Sun, the more neutral coloured Centaurs should be found (because of enhanced coma activity), this correlation may be overruled by the individuality of the objects: 5145 Pholus, having a similar perihelion distance as 2060 Chiron and a similar aphelion distance as 10199 Chariklo, is the reddest Centaur known so far, while Chiron and Chariklo appear to be of neutral or only slightly reddish colour. This may indicate that a thick reddish crust may have formed on the surface of Pholus by high-energy radiation processing of the surface materials and neither impacts nor cometary activity happened over the last couple of million years, the typical dynamical life time of objects in Centaur orbits (Levison 2001).

Since TNOs, namely Cubewanos, orbit the Sun at larger distances (i.e. they should experience less internal activity), but in the more populated Edgeworth-Kuiper Belt region (i.e. they are exposed to more collisions), their surface colours may be the result of a rather complex balance of impact and activity resurfacing on one and radiation reddening on the other side. Assuming for instance a much longer resurfacing time scale than for Centaurs, the colour gradient distribution of Cubewanos would show – on the average – more redder objects than the Centaurs' one. This can explain the "red-shifted" peak in the gradient statistics of Cubewanos as compared to the Centaurs.

In other words: a "blue-shifted" Centaur population (ignoring extreme cases like Pholus and Nessus) as compared to the Cubewanos suggests that activity resurfacing plays a much larger role for the Centaurs than for the latter objects. Since Centaurs are believed to be sunward migrating TNOs, this scenario also implies that TNOs change colours when becoming Centaurs (trend to neutral colours).

Plutinos show a similar gradient statistics as Centaurs. Whether this implies that the bluish colours are produced mostly through the same process as proposed for Centaurs (i.e. cometary activity), is uncertain. At least in one Plutino, Pluto itself, a thin atmosphere is known to form during its perihelion period.

The situation is completely unclear for the scattered disk objects. From the few objects observed no firm conclusion should be drawn and further observations are urgently needed.

In summary: the scenario for the colour evolution path of TNOs towards Centaurs is built on very weak trends in the gradient and colour distributions of these objects. Due to the low number statistics in both cases they are to be considered as uncertain and very speculative for the time being. In particular, more Centaurs need to be measured to put the colour statistics of these objects on safer grounds. The same applies for Plutinos and scattered disk objects.

## 6. Conclusions

Over the past 2 years we have collected photometric data of 16 TNOs and 1 Centaur plus spectra of 5 TNOs. The photometry contributed mostly to the existing data set in the visible wavelength range.

Spectroscopy: with our spectra the number of objects with visible reflectance spectra published is more than doubled. The spectroscopy delivered featureless spectra with spectral gradients which confirm – in principle – the correctness of spectral gradient estimates from broadband filter photometry. The flattening of the object reddening towards the near-IR starts beyond 750–800 nm. Because of $S/N$ limitations no spectral feature specific for a particular surface chemistry was found. Much longer integration times with 8–10 m class telescopes are needed for a search of emission and absorption features in the visible spectra of TNOs and Centaurs. However, because of the assumed surface chemistry (mostly clean and/or radiation processed ices) chances for detections of spectral features are much higher in the near-IR wavelength range.

The colour gradients obtained from spectroscopy are considered to be more reliable than the photometric gradients since they typically fit many wavelength points (not just 4 as for the broadband $BVRI$ photometry). Colour corrections due the rotation light curve are not important. Spectroscopy has longer exposure times (factor of 2–4)

than photometry which makes the use of the largest telescopes a nearly indispensable requirement. Spectral slope changes with rotation phase, however, may be difficult to detect with spectroscopy because of the long integration time for good $S/N$ spectra (in particular for fainter objects). Spectroscopy should certainly be applied for objects which show unusual colour gradients or photometric slope changes (like 1994ES2 and 1994EV3) in order to get wavelength resolved information on these features.

Photometry: the overall colour range of TNOs (Cubewanos, Plutinos, scattered disk objects) and Centaurs in the visible wavelength range seems to be well established. However, the statistical significance of different populations among TNOs and Centaurs is not yet proven based upon the existing set of broadband colours. The spectral gradient population of TNOs and Centaurs may be different, although the number of Centaurs, scattered disk objects and – to a less extend – Plutinos with accurate photometry measured is low. That makes such conclusions somewhat uncertain. However, if confirmed by colour data of a larger sample, the colour gradient diversities between TNOs and Centaurs and among the Centaurs can be indicative for the relative importance of the various resurfacing processes proposed for both object classes.

Obviously, there is a lack of near-IR colour data for all object classes. At present, the existing broadband photometry in the visible is of little use for guidance in the selection of objects that may have interesting surface chemistry.

The existing data set of Cubewanos has already revealed outlyers, i.e. objects which clearly deviate from the typical colour range of TNOs. These TNOs may be interesting targets for spectroscopic follow-up observations which should allow to get a broader and more detailed characterisation of the peculiarity of these objects.

*Acknowledgements.* The observations in August 1998 were part of the VLT Science Verification (SV) program and were executed in service mode by the VLT SV team. We thank the VLT SV team (R. Gilmozzi, B. Leibundgut, J. Spyromilio, K. Virenstrand, A. Walander) for their great work and support in getting our proposal done.

The observations in May and December 1999 were part of the FORS1 Guaranteed Time Observing (GTO) program. We thank the FORS principle investigator, Prof. I. Appenzeller (Landessternwarte Heidelberg) and his instrument team with scientists, engineers and workshop people from the Landessternwarte Heidelberg, the Universitäts-Sternwarte Göttingen and the Universitäts-Sternwarte München, for our participation and the friendly help in/during the FORS GTO program.

The support of the telescope and instrument operators N. Hurtado, F. Lecaros, A. Lopez, H. Nunez and G. Martin at the ESO VLT and NTT as well as of U. Thiele, J. Aceituno and S. Pedraz at Calar Alto is also greatly acknowledged.

## References

Barucci, M. A., Lazzarin, M., & Tozzi, G. P. 1999a, AJ, 117, 1929

Barucci, M. A., Doressoundiram, A., Tholen, D., Fulchignoni, M., & Lazzarin, M. 1999b, Icarus, 142, 476

Barucci, M. A., Romon, J., Doressoundiram, A., & Tholen, D. J. 2000, AJ, 120, 496

Barucci, M. A., Fulchignoni, M., Birlan, M., et al. 2001, A&A, 371, 1150

Brown, R. H., Cruikshank, D. P., & Pendleton, Y. 1997, Science, 280, 1430

Brown, R. H., Cruikshank, D. P., & Pendleton, Y. 1999, ApJ, 519, L101

Cruikshank, D. P., Roush, T. L., Bartholomew, M. J., et al. 1998, Icarus, 135, 389

Davies, J. K., Green, S., McBride, N., et al. 2000, Icarus, 146, 253

Doressoundiram, A., Barucci, M. A., Romon, J., & Veillet, C. 2001, Icarus, submitted

Edgeworth, K. E. 1949, MNRAS, 109, 600

Giacconi, R., Gilmozzi, R., & Leibundgut, B., et al. 1999, A&A, 343, L1

Hainaut, O. R., Delahodde, C. E., & Boehnhardt, H., et al. 2000a, A&A, 356, 1076

Hainaut, O. R., Boehnhardt, H., West, R. M., Delahodde, C. E., & Meech, K. E. 2000b, ESO Conf. Proc., ed. R. M. West, & D. Jewitt, 65

Jewitt, D., & Luu, J. 1998, AJ, 115, 1667

Kuiper, G. P. 1951, in Astrophysics, ed. J. A. Hyne (McGraw-Hill, New York), 357

Landolt, A. 1992, ApJ, 103, 340

Levison, H. F. 2001, IAU Joint Discussion 4, in: Highlights in Astronomy, ed. H. Rickman, in press

Luu, J., & Jewitt, D. 1996, AJ, 112, 2310

Meeus, J. 1998, Astronomical Algorithms (Willmann-Bell Inc., Richmond, USA)

Meech, K. J., Buie, M. W., Samarasinha, N. H., Mueller, B. E. A., & Belton, M. J. S. 1997, AJ, 113, 844

Noll, L. S., Luu, J., Gilmore, D. 2000, AJ, 119, 970

Sekiguchi, T., Boehnhardt, H., Delahodde, C. E., & Hainaut, O. 2001, A&A, submitted

Shul'man, L. M. 1972, in The Motion, Evolution of Orbits, and Origin of Comets, ed. Chebotarev et al., IAU Symp. 45 (Reidel Dordrecht), 265

Stern, S. A. 1995, AJ, 110, 856

Tegler, S. C., & Romanishin, W. 1998, Nature, 392, 49

Tegler, S. C., & Romanishin, W. 2000, Nature, 407, 979

Trujillo, C. A., Jewitt, D., & Luu, J. 2000, BAAS, 32, 2004

Wyckoff, S. 1982, in Comets, ed. L. L. Wilkening (Univ. Arizona Press), 3